PREPARATION AND PHASE CHARACTERISTICS OF AUTOCLAVED AERATED CONCRETE USING IRON ORE TAILINGS

XIAO-YING LIANG[1], DONG-XIA YUAN[1], JUN LI[1], CHANG-LONG WANG[2,1,3] *, XIAO-RAN LIN[1], NING CHANG[1]

[1]School of Civil Engineering, Hebei University of Engineering, Handan Hebei Province, 056038, China.
[2]Jiangxi Key Laboratory of Mining Engineering, Jiangxi University of Science and Technology, Ganzhou Jiangxi Province 341000, China.
[3]Tianjin Sunenergy Sega Environmental Science & Technology Co. Ltd, Tianjin 300000, China.

Based on the background that large amount of iron ore tailings (IOT) are stockpiled in China, the utilization of iron ore tailings to prepare autoclaved aerated concrete (AAC) was studied. The AAC samples were prepared on a laboratory scale with with a bulk density of 588 kg·m^{-3}, compressive strength of 4.82 MPa, and thermal conductivity of 1.50 W/(m·K) which was in line with the requirement of A3.5, B06-class AAC products regulated by autoclaved aerated concrete building blocks (GB 11968-2006). The optimal grinding time of iron ore tailings was 25 min. The AAC samples after autoclaving were examined by using XRD (X-ray diffraction analysis), SEM (scanning electron microscope) as well as ^{29}Si and ^{27}Al NMR (Nuclear Magnetic Resonance). Results show that the main minerals in the AAC samples are tobermorite-11 Å, C-S-H gels, calcite, anhydrate, ferrotschermakite, quartz, with small amount of other minerals brought in by the iron ore tailings. It was also suggested that most minerals in the iron ore tailings participated in the hydration reaction, and the chemical elements in them got into the structure of acicular and platy tobermorite in the subsequent autoclaving process.

Keywords: iron ore tailings; autoclaved aerated concrete; tobermorite; reaction mechanism

1. Introduction

Autoclaved Aerated Concrete (AAC) is a cellular building materials, which provides high thermal efficiency, superior fire resistance and excellent acoustical absorbing abilities [1]. It can be used as a substitution for fired clay brick with the benefits for farmland conservation, environmental protection, and energy saving [2]. The basic ingredients of AAC are calcareous materials (cement and lime) and siliceous materials (silica sand or recycled fly-ash), and an expansion agent—aluminum powder [3].

China has become the largest steel producer in the world. This brings about 7 billion tons of IOT every year, and the comprehensive utilization ratio of IOT is not more than 10% [4]. The accumulation of the tailings has taken large areas of land for storage, and results in server environmental and safety problems [5]. One of the important utilizing tailings routes is to produce building materials, such as cementitious materials or cement [4, 6], autoclaved bricks [7], high-strength concrete [8], glass ceramic [9] and so on. The fine-grained IOT particles gained by crushing, grinding and milling includes a large number of silicate minerals, which has great difference in some respects of chemical and physical properties compared with conventional acidic

materials used to produce AAC materials, the active components in silicate minerals such as SiO_2 and Al_2O_3 are easy to carry on hydration reaction at high temperature and high pressure and produce hydrate calcium silicate hydrates [10]. To reduce the production costs and expand the limit of raw materials, some researchers have investigated the probability of substituting the conventional raw materials of AAC by industrial waste, such as air-cooled slag [11], phosphorus slag and efflorescence sand [12], coal bottom ash [13], lead–zinc tailings [14] and copper tailings [15]. Using tailings as a supplement for artificial or natural sand to produce AAC is a promising way to solve the sand resource shortage problem and the environmental problems caused by the tailings. Mechanical grinding of IOT has been adopted to decrease their particle size and improve their chemical activity when they are used as siliceous materials in AAC.

In this study, IOT was used as mainly raw materials to prepare AAC. The object of the present work is to investigate the grinding characteristic of IOT, microstructural properties and phase compositions of the AAC prepared by IOT, and to make primary understanding of reaction mechanism during the process of autoclaving, especially the behavior of IOT in the hydrothermal reaction.

---

* Autor corespondent/*Corresponding author*,
E-mail:13716996653@139.com

Table 1

Chemical composition of raw materials (wt. %)

Materials	SiO_2	Al_2O_3	Fe_2O_3	FeO	MgO	CaO	Na_2O	K_2O	SO_2	Loss
IOT	68.96	7.68	2.32	4.47	3.64	4.35	1.41	1.85	0.024	2.49
L	5.45	3.85	1.68	0.08	3.56	78.76	—	1.25	0.45	3.93
OPC	25.06	6.10	3.31	0.21	3.87	55.56	0.23	0.95	—	4.16
FGDW	2.84	0.78	0.25	0.03	0.47	40.13	0.14	0.12	33.21	—

2. Materials and methods

2.1. Experimental materials

The AAC samples were prepared using the following raw materials: IOT, lime (L), 42.5 ordinary Portland cement (OPC) and the gypsum of flue gas desulfurization waste (FGDW). The chemical compositions of the raw materials are listed in Table 1.

IOT. Table 1 shows that the amount of SiO_2 in the IOT was approximately 68.96 %, and the level of residual iron in the tailing, which was present in the form of magnetite, was approximately 5.2 %. The IOT thus were of a low-silicon high-iron magnetite-quartzite type. The 0.08 mm sieve residual of IOT was 65.28%.

OPC. The cement used was ordinary Portland cement with the strength grade of 42.5 which complies with the Chinese National Standard GB 175–1999.

L. The content of effective CaO was 71%. The digestion time of L was 15 min, and the digestion temperature was 65 ºC. The 0.08 mm square hole sieve residual of L was less than 12 %.

FGDW. The primary mineral phase of FGDW is $CaSO_4 \cdot 2H_2O$. The specific surface area of the FGDW is 389 m^2 kg^{-1}, and 0.08 mm sieve residual is less than 7.9%.

2.2. Experimental Method
2.2.1. Preparation of AAC

Firstly, IOT was dried in oven (DH-101) at 105 ºC for 24 h to make moisture content less than 1wt%, and then ground with the SM Φ500 mm×500 mm 5 kg small ball grinder at the speed of 48 r·min⁻¹. The grinding periods were chose at 15 min, 20 min, 25 min, 30 min, 35 min and 40 min in order to obtain different surface area. According to the grinding periods, the obtained ground samples were labeled as G_{15}, G_{20}, G_{25}, G_{30}, G_{35}, G_{40}, respectively.

The materials were mixed at the designed proportions, and the solid mixture was blended with water at w/s ratio of 0.55 for 1 min, with addition of 0.55% aluminum powder. Mixture slurry was then molded in 100 mm×100 mm×100 mm for compressive strength test. After demolding, the specimens were subjected to two curing steps. At the first step, specimens were heated in furnace at 70 ºC for 2 h to achieve the desired setting and volume stability and then autoclave curing was conducted under 12.5 bars and 185 ºC steam pressure for 8 h. At the end of the curing period, the autoclave was cooled down slowly until it reached the room temperature.

2.2.2. Sample characterization

The bulk density, compressive strength and thermal conductivity (TC) of the AAC samples were measured according to Chinese standard GB/T 11968-2008 *Autoclaved aerated concrete blocks.* TC of AAC samples was measured using a VQ-300 measuring instrument with determination range from 0.01 to 1.50 W/(m·K). The X-ray diffraction (XRD) spectra of AAC samples were performed using a D/Max-RC diffractometer (Japan) with Cu Kα radiation, voltage of 40 kV, current of 150 mA and 2θ scanning ranging between 5 º and 90 º. SEM observation was performed to analyse the microstructure of samples using a Zeiss SUPRA™55 scanning electron microscope coupled with a Be4-U92 energy spectrum. The ²⁹Si and ²⁷Al magic angle pattern were obtained using a Bruker Avance Ⅲ400 Solid Nuclear magnetic resonance, operating at 59.62 MHz for ²⁹Si and 104.0 MHz for ²⁷Al.

In order to compare the compressive strength directly between the samples with different bulk density (BD), a concept of specific strength was introduced. The specific strength (SS) is defined as the ratio of tested compressive strength (CS) to the bulk density of the samples. That is:

$$SS = \frac{CS}{BD} \quad (1)$$

3. Results and Discussion

3.1. Influence of fineness of IOT on AAC properties

Fig. 1 showed the IOT particle size after grinding was polarized and did not follow logarithmic normal distribution.The particle size decreases rapidly after 15 min of powder grinding, leaving over 50% of particles smaller than 10 μm. As the powder grinding persists, fewer and fewer particles remain larger than 10 μm. As shown in the figure, submicron particles were produced, taking up 3.20 % of the IOT particles, at 15 min of powder grinding; the proportions of submicron particles kept growing and end up at 3.39 %, 3.50 %, 3.53 %, 5.07

Table 2

Effect of fineness of IOT on the casting stability and properties of AAC samples

Grinding time/min	Slurry fluidity	Casting stability	BD/(kg·m^{-3})	CS/MPa	SS/m
G$_{15}$	poor	bubbling	612	3.98	6.50
G$_{20}$	general	good	603	4.15	6.88
G$_{25}$	good	good	595	4.71	7.92
G$_{30}$	good	preferably	596	4.65	7.80
G$_{35}$	preferably	preferably	608	4.48	7.37
G$_{40}$	preferably	slightly bubbling	623	4.24	6.81
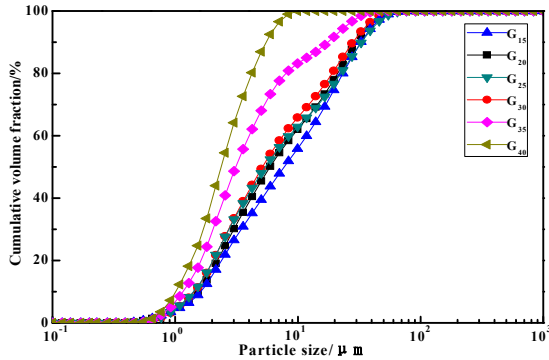
Fig.1- Relationship of particle size distribution and grinding time.

% and 7.24 %, respectively, with the increasing of the duration of powder grinding. It was shown that IOT particles were gradually refined during the powder grinding process, and the increasing of the grinding time promotes the decrease of the IOT particle size.

The specific surface area of the samples of G$_{15}$, G$_{20}$, G$_{25}$, G$_{30}$, G$_{35}$ and G$_{40}$ were respectively 227.73 m^2·kg^{-1}, 275.60 m^2·kg^{-1}, 311.25 m^2·kg^{-1}, 335.37 m^2·kg^{-1}, 384.76 m^2·kg^{-1} and 428.81 m^2·kg^{-1} respectively. The specific surface area of IOT increased rapidly at the early stage of grinding. The grinding time was from 15 min to 25 min, and the specific surface area was increased by 26.83 %. However, the grinding time increased from 25 min to 30 min, and the specific surface area only increases by 7.19 %. Due to the phenomenon of weak agglomeration in grinding 25 min, the specific surface area changed little, which corresponds to the change of particle size distribution (See Fig.1). Therefore, in terms of energy conservation and cost, IOT used in this study should be controlled at 25 min grinding time when used as the siliceous materials in the AAC production.

Table 2 displayed BD, TCS and SS of AAC samples and related raw materials ratio. In all the samples, the content of FGDW gypsum was 5 wt%. As shown in Table 2, the largest TCS and SS of sample was obtained when it contains 60 % IOT, 25 % L, 10 % OPC and 5 % FGDW. The effect of fineness of IOT on the casting stability and the properties of AAC samples were given in Table 2. The Table 2 indicated that longer grinding time favored the increase of samples' CS. The reason was that with the extension of grinding time, more and more reactive species (ions or free radicals) was exposed to the surface, which made the

reaction with other components in the system easily. The results showed more and more hydration products were formed, which played an important role to the development of strength. The best SS value (up to 7.92 m) was obtained when the grinding time was 25 min. However, after 25 min, the special compressive strength of AAC declined with the increasing of grinding time. Too short or too long grinding time was unhelpful to the strength development. It was because, as the fineness of IOT declined, the fluidity of slurry in the casting mold improved and numerous fine and even foams form, lowering BD. On the other hand, extra fine IOT enlarged the slurry fluidity greatly that low fluidity may cause breakage of numerous foams during the casting process, thus led to an improved BD. The finer the IOT, the larger the surface reacting particles would be provided. This broadened the contact area between Ca(OH)$_2$ and soluble matters on the surface of the IOT, improved their reaction speed and generating more hydration production. In this way, the AAC strength increased. On the other hand, extra fineness (below dozens of microns) caused unreacted residues too small that a good foam structure failed to form and strength decreased. So considering casting stability and the properties of AAC samples, the grinding time of IOT was selected for 25 min.

3.2. Influence of content of IOT on AAC properties

Under hydrothermal synthesis, calcareous and siliceous materials undergo a series of physical and chemical changed to turn into AAC, which was mainly composed of hydrated phases such as crystalline tobermorite and hydrated calcium silicate, both of which determined the property of AAC.
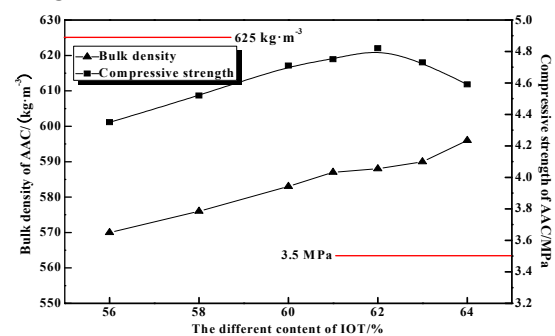

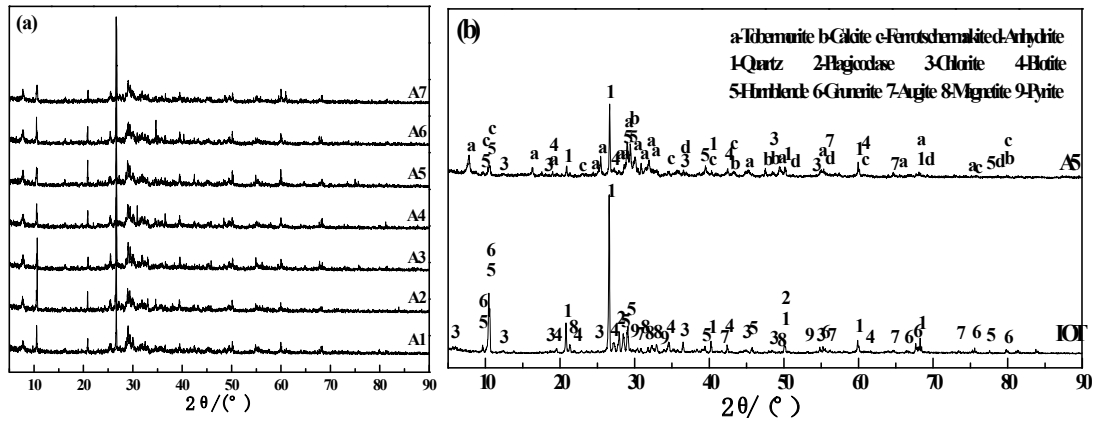Fig. 2- Influence of content of IOT on AAC properties.

Fig. 3 - XRD spectra of AAC samples and IOT, (a)- XRD spectra of AAC samples with different content of IOT; (b) XRD spectra of A5 sample and IOT.

Fig. 2 showed that BD of AAC samples kept growing with the increasing content of IOT, when the content of IOT was 64 %, BD of A7 sample was the largest, reaching 596 kg·m^{-3}. CS of AAC samples also first increased and then decreased with the increasing content of IOT, peaking at a value of 4.82 MPa by A5 with IOT content of 62 %, which has reached the requirements of AAC prepared from sand or fly ash (The line in Fig. 2 was the BD and CS required by the standard GB 11968-2006).

Fig. 3(a) and Fig. 3(b) showed the XRD spectra of AAC samples and original IOT. The curve of original IOT in Fig. 3(b) identified that most of the minerals were well crystallized, which suggested by the sharp diffraction peaks and low back ground. The main minerals phases were quartz, hornblende, grunerite and plagioclase, accompanied by minor phases including augite, biotite, chlorite, pyrite and magnetite. It can be seen that the major minerals in the final AAC sample were tobermorite-11 Å, anhydrite, hornblende, ferrotschermakite and residual minerals quartz, accompanied by calcite, chlorite, biotite and augite in minor quantities. Comparing spectra of IOT and AAC, the characteristic peaks of quartz decreased significantly, meanwhile plagicoclase from IOT was not detected. That was to say the minerals in IOT was evidently involved into the hydrothermal reaction during the 8 h autoclaving process. AAC Body autoclaved beginning stages, the insufficient amount of dissolved Si^{4+} ions and Al^{3+} ions from IOT were present with an excessive amount of Ca(OH)$_2$, resulting in the formation of a small amount of tobermorite-11 Å. As the autoclaving time extended, a large amount of Si^{4+} ions and Al^{3+} ions were dissolved from IOT in alkaline hydrothermal conditions, which promoted the formation of tobermorite. Meanwhile, the disappeared intensity of the plagicoclase indicated that more tobermorite formed and Ca(OH)$_2$ was depleted during the autoclaving since the diffraction peaks of tobermorite displayed an increasing trend. As indicated in AAC's spectrum, most minerals of pyrite and magnetite in IOT were not detected. The non-

detection of magnetite and pyrite was likely due to the fact that the overall amount of those minerals originally comprising small amount in IOT were in more minor quantities after addition into the dry mixture, so that the XRD was not sensitive enough to allow detection at such low level. At the same time, the broad band at around of "convex closure". in two theta range between 26–34 ° indicated that there is amorphous diffraction (no) of amorphous and low crystallized C-S-H gels. The ferrotschermakite phase in the AAC products was a double chain structure, the reason was due to the grunerite in IOT occured ion exchange between Al^{3+}, Si^{4+}, Ca^{2+} and Fe^{2+} through autoclaving process. Calcite also occurred in the AAC products, which was a frequently encountered phase in most of the calcium-rich building materials formed by absorbing CO$_2$ in the atmosphere. The calcite, ferrotschermakite, anhydrite together with non-reacted hornblende, biotite, chlorite augite and residual minerals quartz would become the primary aggregate in the AAC samples.

Fig.4 showed the microstructure of AAC samples after autoclaved for 12 h which were mainly tobermorite and C-S-H gels. Due to the increasing amount of IOT, tobermorite in the in the stomata increased, turning from needle shapes (A1(a) and A2(c)) into short fibrous shape (A5(i)). The tobermorite then cross with each other to create a good network structure, so that CS of the samples increased. But the shape of the tobermorite will possibly change back to a needle shape if there were too many IOT. Under this circumstance, tobermorite will become loose, so that BD was reduced. Most of the hydrated products in the cross section were low crystallinity and noncrystalline C-S-H gels, which glued to fibrous or schistose tobermorite so that the amount of tobermorite with a good crystallite shape was reduced (A1(b), A2(d) and A7(n)) and the CS of the samples reduced. At the same time, IOT particles will gradually escape from the coverage of decreasing tobermorite because of the extra high amount of IOT. Thus the network structure
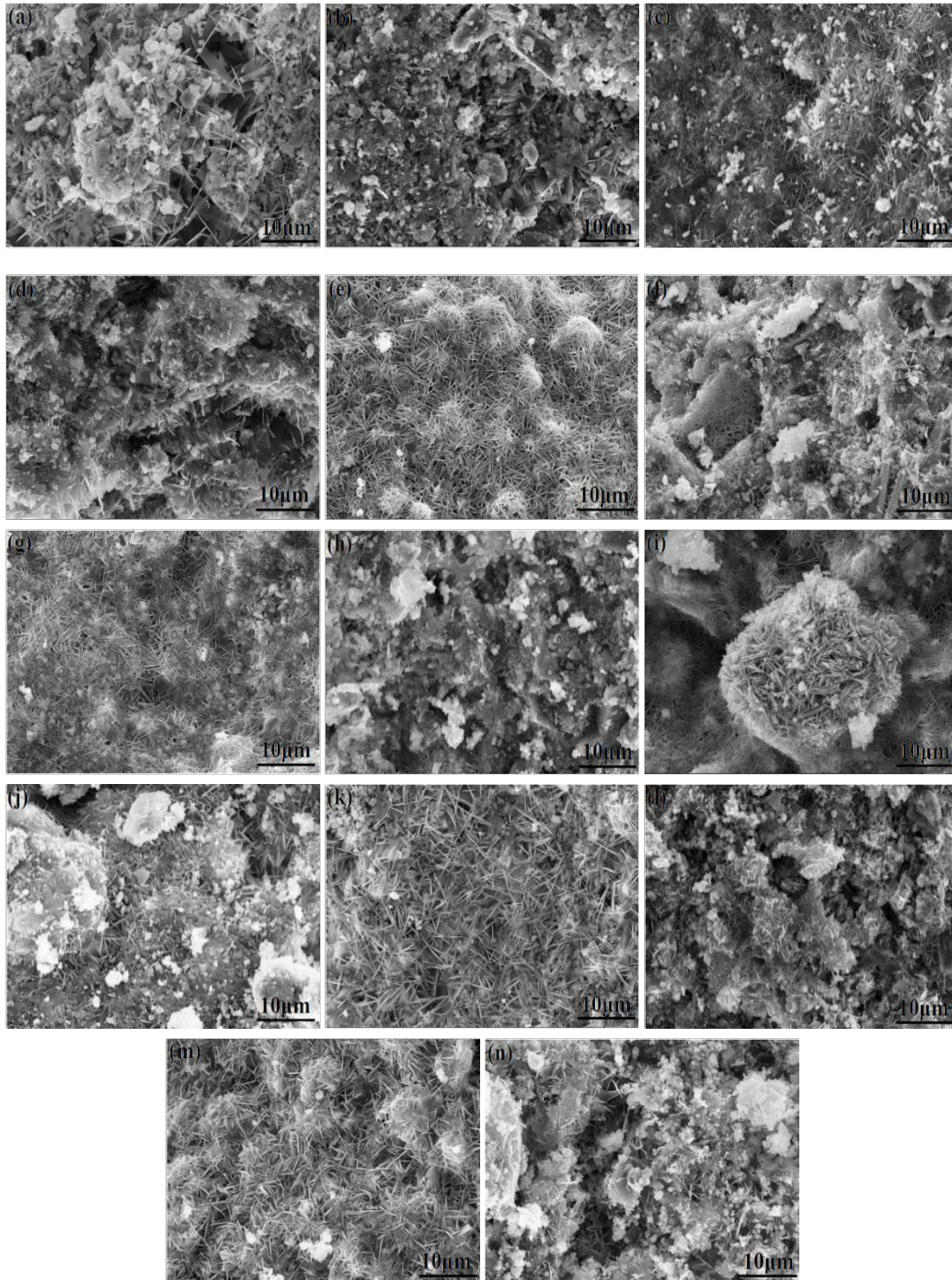
Fig. 4 - SEM images of the hydration products for AAC of different IOT content, the hydration products in the stomata for A1(a), A2(c), A3(e), A4(g), A5(i), A6(k) and A7(m); the hydration products of cross-section for A1(b), A2(d), A3(f), A4(h), A5(j), A6(l) and A7(n).

loosened and CS reduced. The fluidity of slurry lowered, and there was uneven foam structure in the casting body. The swelling height of the body was too low, and tiny cracks even emerge along the vertical path of gas emission of A7 with 64% IOT content. BD, CS and TC of A5 with 62% content was 588 $kg \cdot m^{-3}$, 4.82 MPa and 1.50 $W/(m \cdot K)$, respectively.

3.3. ^{29}Si and ^{27}Al NMR analysis of AAC

The ^{29}Si NMR spectra of IOT and the final AAC samples was given in Fig.5. Two major peaks at chemical shift of -96.6×10^{-6} and -99.8×10^{-6} were observed on ^{29}Si NMR spectrum of IOT in the Fig.5 (a), which were originated from the hornblende or grunerite. It showed that there were two major tetrahedral structure states of Q^4 (1Al) and Q^4 (2Al) in the hornblende or grunerite particles. It was well known that hornblende or grunerite could have a wide range of Si/Al ratio, where calcium-rich hornblende or grunerite would need more aluminum to balance the electric charge, and calcium-poor hornblende or grunerite would need less aluminum to balance the electric charge. The peak at chemical
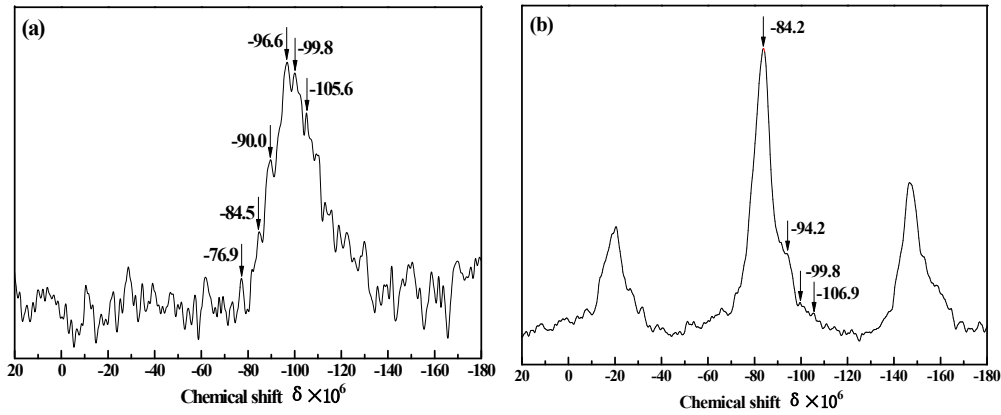
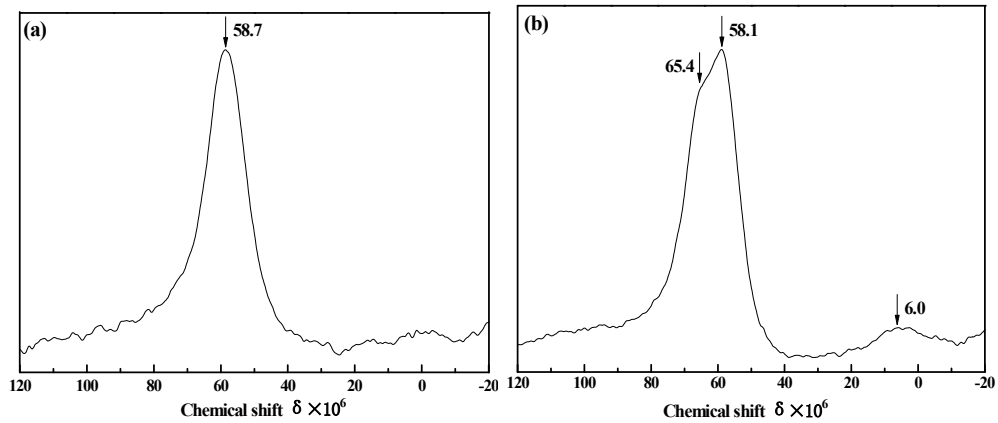**Fig. 5** - 29Si NMR spectra of IOT and AAC sample, (a)-IOT; (b)-AAC of A5 sample.

Fig. 6 - 27Al NMR spectra of IOT and AAC sample, (a)-IOT; (b)-AAC of A5 sample.

shift of -105.6×10^{-6} represented a typical tetrahedral structure state of Q^4, which could be attributed to quartz. The peak at chemical shift of -90.0×10^{-6} may be caused by the overlap of two tetrahedral structure states of Q^3 [n Al (n<1)] and Q^4 (3Al). The Q^4 (3Al) was attributed to the calcium-rich plagioclase. This may be because IOT in this study belonged to magnetite-quartz type, which was consistent with its chemical composition. The tetrahedral structure state of Q^3 [n Al (n<1)] was attributed to hornblende or grunerite. The peak at chemical shift of -84.5×10^{-6} was an indicative of Q^3 [n Al (n<1)], which could be belong to biotite and chlorite. Tetrahedral structure state of Q^2 was showed the peak at chemical shift of -76.9×10^{-6}, which could be assigned to augite. Thus, the mineral phase of IOT detected by XRD corresponded to the tetrahedral structure states of silicon showed by the major peaks and subsidiary peaks of the 29Si NMR spectrum of IOT.

Fig. 5(b) indicated the 29Si NMR spectrum of AAC, corresponding to A5 sample. As shown in Fig. 5(b), the peak was sharp, its left shoulder was smooth and deep, right shoulder was widening with three subsidiary peaks. The major peak at chemical shift of -84.2×10^{-6} was indicative of Q^3 tetrahedral structure state which Al was not replaced by other atoms. And some the iron-bearing minerals in IOT disappeared as shown in Fig. 5(b). These results suggested that most of Fe^{3+} had been combined into

some newly formed phases in the AAC of A5 sample. It was possible that some Fe^{3+} insert tobermorite structure to substitute Al^{3+} in the double chain [16]. If this happened, the peak toward larger negative value would occur. The reason was that Fe^{3+} has much higher electro negativity value (1.83) than Al^{3+} (1.61). The Fe tetrahedrons would contribute fewer electrons to the nearby Si atoms than the Al tetrahedrons. In such a case, the peak at chemical shift of -84.2×10^{-6} in Fig. 5(b) may be indicative in Q^3 (n (Al, Fe)), with n≈1. Fig. 5(b) also showed that the peaks at chemical shift of -94.2×10^{-6} and -99.8×10^{-6} were apparently attributed to non-reacted hornblende or Ferrotschermakite produced by ion replacement after autoclaved and the peak at -106.9×10^{-6} was attributed to residue quartz. This suggested that most of the quartz particles and plagioclase particles had been consumed during the autoclaving hydrothermal reaction. This seemed to be in contradiction with that shown in Fig. 3, where quartz diffraction peak was still existing in the XRD spectrum.

Fig. 6(a) was 27Al NMR spectrum of IOT. As shown in in Fig. 6(a), only a peak at chemical shift of 58.7×10^{-6} was detected. It suggested that all of the Al atoms in IOT were in the structural state of tetrahedral coordination. A further indication was that almost all of Al atoms in IOT were in the silicate tetrahedral networks or chains, as a substitution of Si atoms.

Fig. 6(b) showed the ^{27}Al NMR spectrum of AAC corresponding to A5 sample. It was shown that a major peak at 58.1×10^{-6}, a minor peak at 6.0×10^{-6} and a subsidiary peak at 65.4×10^{-6} were detected.

Both the major peak at chemical shift of 58.1×10^{-6} and the subsidiary peak at chemical shift of 65.4×10^{-6} were indicative of structural state of tetrahedral coordination for Al, but they suggested two different condition. It was expectable that some Al tetrahedrons were actually hydrolyzed in the newly formed phase, which would lowered the electron density of the related Al atoms due to the positive charge of the hydrogen ions, this would lead to the chemical shift toward a smaller value. The peak position changed from 58.7×10^{-6} to 58.1×10^{-6} by compare Fig. 6(a) and (b). On the other hand, some aluminum tetrahedrons may not be hydrolyzed, but in the structure of silicate-aluminum tetrahedral chains such as tobermorite, rather than three dimensional networks, such as plagioclase. Such a change would lead to an increase of electron density of Al atoms, and subsequently leading to chemical shift changed from 58.7×10^{-6} to 65.4×10^{-6}.

The above analysis suggested that during autoclaving process under 12.5 bars and 185 ºC steam pressure for 8 h. Most of quartz and plagioclase particles were also decomposed. The decomposed compositions were mostly combined into newly formed phases including tobermorite and other calcium aluminum silicate hydrates. So, these newly formed phases were relatively iron-rich compared with the traditional AAC materials, which may leaded to the waving curved morphology of tobermorite and other minerals. The decomposed sulphate ions and calcium ions formed anhydrite, and some aluminum was recombined into silicate phases in the structural state of tetrahedral coordination.

4. Conclusions

(1) It is feasible that iron ore tailings could be used as substitutional siliceous materials of fly ash and quartz sand to produce AAC. This may develop a way to utilize iron ore tailings for reuse.

(2) The AAC sample with a bulk density of 588 kg·m^{-3} and compressive strength of 4.82 MPa was produced by the raw material composition of 62 % iron ore tailings, 24 % lime, 9 % ordinary Portland cement, 5 % the gypsum of flue gas desulfurization waste.

(3) The main minerals in the AAC were acicular and platy tobermorite-11 Å, C-S-H gels, calcite, anhydrite, ferrotschermakite besides quartz and other residual minerals from the iron ore tailings. Through the NMR analysis, it could be find that in the tobermorite structure, some the iron-containing minerals in the iron ore tailings were decomposed during the autoclaving hydrothermal

reaction and iron atoms and other atoms were transferred into the newly form phases including tobermorite, which may resulted in the waving-curved morphology of these acicular and platy crystals.

REFERENCES

1. X.W. Cui, C.L. Wang, W. Ni, Y.Q. Di, H.L. Cui and L. Chen, Study on the reaction mechanism of autoclaved aerated concrete based on iron ore tailings, Romanian Journal of Materials, 2017, **47**(1): 46.
2. T. Piyush, Energy efficiency and building construction in India, Building and Environment, 2001, **36**(10), 1127.
3. S. Torsten, New insights regarding sound protection with autoclaved aerated concrete, Concrete Precasting Plant and Technology, 2004, **70**(2), 136.
4. Z.L. Yi, H.H. Sun, X.Q. Wei and C. Li, Iron ore tailings used for the preparation of cementitious material by compound thermal activation, International Journal of Minerals, Metallurgy and Materials, 2009, **16**(3), 355.
5. C. Reid, V. Bécaert, M. Aubertin, R.K. Rosenbaum and L. Deschênes. Life cycle assessment of mine tailings management in Canada, Journal of Cleaner Production, 2009, **17** (4), 471.
6. C. Li, H.H.Sun, Z.L. Yi and L.T. Li, Innovative methodology for comprehensive utilization of iron ore tailings: Part 2: The residues after iron recovery from iron ore tailings to prepare cementitious material, Journal of Hazardous Materials, 2010, **174**(1-3), 78.
7. Y.L. Chen, Y.M. Zhang, T.J. Chen, Y.L. Zhao and S.X. Bao, Preparation of eco-friendly construction bricks from hematite tailings, Construction and Building Materials, 2011, **25**(4), 2107.
8. T.I. Ugama, S.P. Ejeh and D.Y. Amartey, Effect of iron ore tailing on the properties of concrete, Civil and Environmental Research, 2014, **6**(10), 7.
9. U.P. Arunachalam, M. Edwin,Theoretical investigation of a ceramic monolith heat exchanger using silicon carbide and aluminium nitride as heat exchanger material, International Journal of Heat and Technology, 2017, **35**(1), 645.
10. C.L. Wang, W. Ni, S.Q. Zhang, S. Wang, G.S. Gai and W.K. Wang, Preparation and properties of autoclaved aerated concrete using coal gangue and iron ore tailings, Construction and Building Materials, 2016, 104(1), 109.
11. X.W. Cui, Ni W. Wen, C. Ren, Early hydration kinetics of cementitious materials containing different steel slag powder contents, International Journal of Heat and Technology, 2016, **34**(4), 590
12. B.G. Ma and Z. Xu, Study on a new kind of aerated concrete containing efflorescence sand-phosphorus slag-lime, Journal of Building Materials, 1999, **2**(3), 223.
13. N. Narayanan and K. Ramamurthy, Structure and properties of aerated concrete: a review, Cement and Concrete Research, 2000, **22**(5), 321.
14. G. Lin, C. L. Wang, C. Y. Qiao, H. L. Cui, L. Chen and S. Yu, Preparation and properties of autoclaved aerated concrete containing lead-zinc tailings, Romanian Journal of Materials, 2016 , **46** (3), 334.
15. X.Y. Huang, W. Ni, W.H. Cui, Z.J. Wang and L.P. Zhu, Preparation of autoclaved aerated concrete using copper tailings and blast furnace slag, Construction and Building Materials, 2012, **27**(1), 1.-5.
16. N.Y. Mostafa, E.A. Kishar and S.A. Abo-El-Enein, FTIR study and cation exchange capacity of Fe^{3+} - and Mg^{2+} - substituted calcium silicate hydrates, Journal of Alloys and Compounds, 2009, **473**(1), 538.

****